Severe plastic deformed Pd-based metallic glass for superior hydrogen evolution in both acidic and alkaline media

Fei Chu [a], Bin Han [a], Kaveh Edalati [b], Jiang Ma [c], Yuying Meng [a], Chao Wang [d], Fan Yang [d], Peng Zhang [a], Huai-Jun Lin [a,*]

[a] *Institute of Advanced Wear & Corrosion Resistance and Functional Materials, Jinan University, Guangzhou 510632, China*
[b] *International Institute for Carbon-Neutral Energy Research (WPI-I2CNER), Kyushu University, Fukuoka 819-0395, Japan*
[c] *Guangdong Provincial Key Laboratory of Micro/Nano Optomechatronics Engineering, College of Mechatronics and Control Engineering, Shenzhen University, Shenzhen 518060, China*
[d] *Institute of Physics, Chinese Academy of Sciences, Beijing 100190, China*

ARTICLE INFO

ABSTRACT

The electrocatalytic hydrogen evolution reaction (HER) on a $Pd_{40}Cu_{30}Ni_{10}P_{20}$ metallic glass (MG) in both acidic and alkaline media is enhanced through severe plastic deformation using high-pressure torsion (HPT). The severe plastic deformation increased the energy state of the sample by approximately 21.7J/g without causing crystallization. The overpotentials at 10 mA cm^{-2} of the HPT-treated $Pd_{40}Cu_{30}Ni_{10}P_{20}$ MG are 76 mV and 209 mV in 0.5 M H_2SO_4 and 1.0 M KOH, respectively, which are much smaller than those of 179 mV and 379 mV for the melt-spun $Pd_{40}Cu_{30}Ni_{10}P_{20}$ MG at the same conditions. The improved HER performances should be mainly attributed to the significantly increased density of flow units in the amorphous matrix by severe plastic deformation.

Severe plastic deformation by the high-pressure torsion (HPT) on a $Pd_{40}Cu_{30}Ni_{10}P_{20}$ metallic glass (MG) would generate more flow units upon the amorphous matrix and significantly improve the electrocatalytic hydrogen evolution reaction (HER) performances in both acidic and alkaline media.

© 2021 Acta Materialia Inc. Published by Elsevier Ltd. All rights reserved.

Hydrogen plays an important role in facing the energy crisis as a pollution-free and renewable energy carrier.[1,2] Electrolysis of water is an environmentally friendly, economical and sustainable way to produce hydrogen.[3] However, owning to the sluggish kinetics of hydrogen evolution reaction (HER), which is one of the main reaction of water splitting, efficient catalysts are still needed to accelerate this reaction.[4]

Metallic glasses (MGs), as a group of metastable materials, have showed superior properties compared with their corresponding crystalline alloys due to the unique long-range disordered atomic structure.[5] Additionally, such amorphous structures are beneficial for catalytic performance where more catalytic active sites can be introduced on the surface for electrochemical applications.[6–8] Meanwhile, the dealloying during electrochemical tests could enrich active sites and makes MGs possess unique self-enhanced catalytic activity.[9]

Although the atoms in MGs are uniformly and randomly distributed from a macro point of view, similar to the defects in crystalline materials, there also exist some local domains with inhomogeneous chemical compositions inside the MGs matrix, which could be denoted as flow units.[10,11] Different from the amorphous matrix, the atoms in flow units are more loosely arranged and in higher energy states, which might be beneficial for catalyzing the electrochemical reactions. [10,12]

The properties of MGs can be effectively tuned by changing the density of flow units by different thermal or mechanical methods. Xue et al. showed that the concentration of flow units in MGs can be continuously changed during isothermal annealing.[13] Wagner et al. reported that the amount of flow units can be increased as shear stress enhances.[12] The mechanical properties such as plasticity and toughness of MGs can be effectively improved by adjusting the density of flow units.[14–16] High-pressure torsion (HPT) is an efficient technique for structural modification by combining compression and concurrent torsion [17], which can cause severe plastic deformation and induce abundant flow units and hereby improve the properties of MGs.[18],[19] Edalati et.al reported that the HPT process could effectively enhance the hydrogenation kinetics of Mg-based hydrogen storage alloy.[20] In previous studies, a $Fe_{78}Si_9B_{13}$ MG subjected to the HPT treatment showed enhanced catalytic performance for hydro-
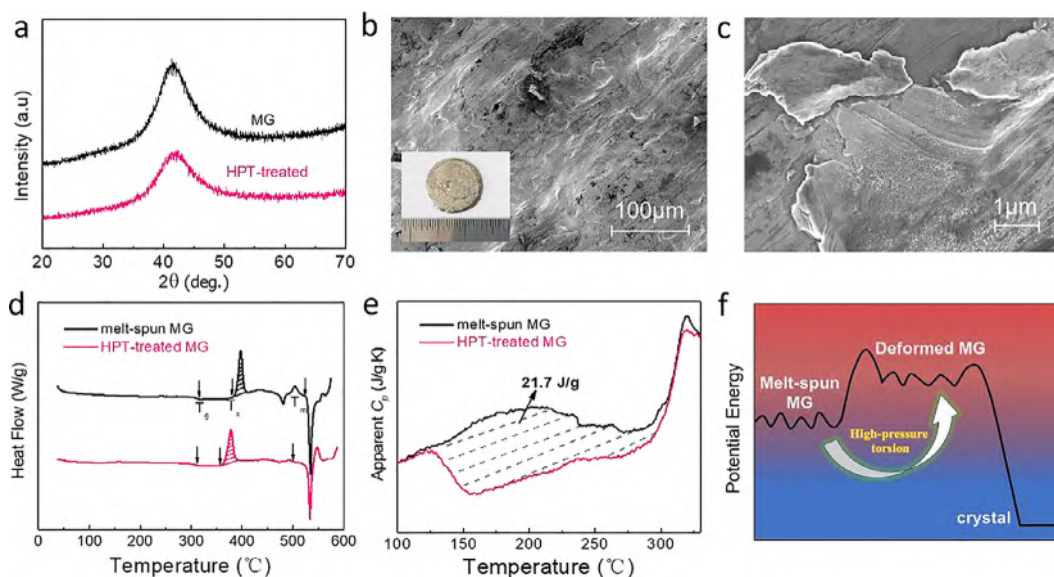
Fig. 1. (a) XRD patterns of the melt-spun and HPT-treated $Pd_{40}Cu_{30}Ni_{10}P_{20}$ MGs; (b and c) SEM images of the HPT-treated MG, insert is the optical picture; (d and e) DSC curves of the melt-spun and HPT-treated $Pd_{40}Cu_{30}Ni_{10}P_{20}$ MGs; (f) a schematic diagram describing the energy state of melt-spun MG and HPT-treated sample.

gen evolution and oxygen evolution.[21,22] However, since the Fe-based MGs are usually quite hard, the HPT treatment would induce nanocrystallization upon the amorphous matrix, and the effect of nanocrystals on the catalytic performance is difficult to elucidate.

In this study, a $Pd_{40}Cu_{30}Ni_{10}P_{20}$ MG, which is much softer than Fe-based MGs, is subjected to HPT treatment and the HER catalytic performances are studied. Results show that the HPT-treated MG without causing obvious crystallization exhibits superior HER catalytic performance in both acidic and alkaline media. The overpotential is 76 mV at 10 mA cm^{-2} in 0.5 M H_2SO_4 and 207 mV at 10 mA cm^{-2} in 1 M KOH, while the overpotentials of MG in the corresponding electrolyte environments are 179 mV and 379 mV, respectively.

The $Pd_{40}Cu_{30}Ni_{10}P_{20}$ MG ribbons were prepared by melt spinning in high-purity argon atmosphere and then they were put into the mold for the HPT treatment at ambient temperature. The HPT parameters were set as follows, pressure of 6 GPa, rotation speed of 1 rpm and rotations of 10 turns. The phase structures of the melt-spun and HPT-treated $Pd_{40}Cu_{30}Ni_{10}P_{20}$ MG were studied by X-ray diffraction (XRD, Rigaku Ultima IV) and the thermal behaviors were studied by using a METTLER 3$^+$ thermal analyzer at a heating rate of 30 K min^{-1}. The microstructures and chemical compositions were studied by scanning electron microscopy (SEM, ZEISS ULTRA 55) attached with an energy dispersive X-ray spectrometer (EDS). X-ray photoelectron spectroscopy (XPS) tests were carried out in a Thermo Scientific Escalab 250Xi with *C 1s* as correction reference. Electrocatalytic performances in acidic and alkaline media were evaluated by using a CHI760E electrochemical workstation with a standard three-electrode configuration at room temperature, in which the melt-spun and HPT-treated MGs were served as the working electrode. The Ag/AgCl electrode and the carbon rod were selected to be the reference electrode and the counter electrode, respectively. 40 segments cyclic voltammogram (CV) cycles were carried out to make the samples to reach a stable state for further electrochemical tests. The linear sweep voltammetry (LSV) was gained with a scan rate of 5 mV s^{-1} for polarization curves. The Tafel slopes were calculated from the LSV curve by using Tafel formula.[23] Electrochemical impedance spectra (EIS) for different samples were measured with an perturbation voltage of 10 mV and a frequency ranging from 100 kHz to 0.1 Hz. Electrochemical surface area (ECSA) was obtained by the double-

Table 1
Glass transition temperature (T_g), onset crystallization temperature (T_x), peak temperature (T_p), melting temperature (T_m) and crystallization enthalpy (ΔH) of melt-spun and HPT-treated MGs.

	T_g (°C)	T_x (°C)	T_p (°C)	T_m (°C)	ΔH (J/g)
MG	312.9	377.4	397.2	521.1	47.62
HPT-treated	312.7	357.6	377.2	500.5	42.05

layer capacitors (C_{dl}) equation (ECSA = C_{dl}/C_{dl-Ref}) where C_{dl-Ref} is 0.04 mF cm^{-2} (the double layer capacitance of a flat surface) and C_{dl} was measured by cyclic voltammogram (CV) at various scan rates. In addition, the two samples were also subjected to 1000 CV cycles in acidic and alkaline media to explore their HER stability. Fig. 1a shows the XRD patterns of the melt-spun and HPT-treated $Pd_{40}Cu_{30}Ni_{10}P_{20}$ MGs. Both of them are amorphous, indicating that the HPT treatment has not led to crystallization, which are very different from our previous study on the Fe-based MGs.[21] This result is the same as we expected, and the effect of nanocrystallzation on HER performance can be got rid of. Fig. 1b and c show the SEM images of the HPT-treated sample and the actual picture is inserted. The surface contains many folds and cracks, which increased its effective contact area in HER catalytic process.[24]

In order to quantify the effect of HPT treatment on the energy state, DSC measurements were performed for melt-spun and HPT-treated MGs at a heating rate of 30 K min^{-1}. Fig. 1d shows that the glass transition temperature (T_g) keeps unchanged after HPT treatment; however, the onset crystallization temperature (T_x) is reduced from 377.4 °C to 357.6 °C and the melting temperature is also approximately decreased about 20 °C. The change of thermal behaviors should be due to the severe plastic deformation caused by the HPT treatment. Moreover, the crystallization enthalpies (ΔH) of the two samples were calculated as listed in Table 1. Combining the changes of T_x and ΔH, it can be concluded that the crystallization behavior of the HPT-treated MG is easier to happen and the energy required for crystallization is reduced. To better reveal the difference in energy states, the DSC curves were calibrated as follows: all curves were brought to zero heat flux at 100 °C because no thermal behavior occurs at this relatively low temperature; then the curves were corrected by using a linear correction to accordant with each other in the supercooled liq-
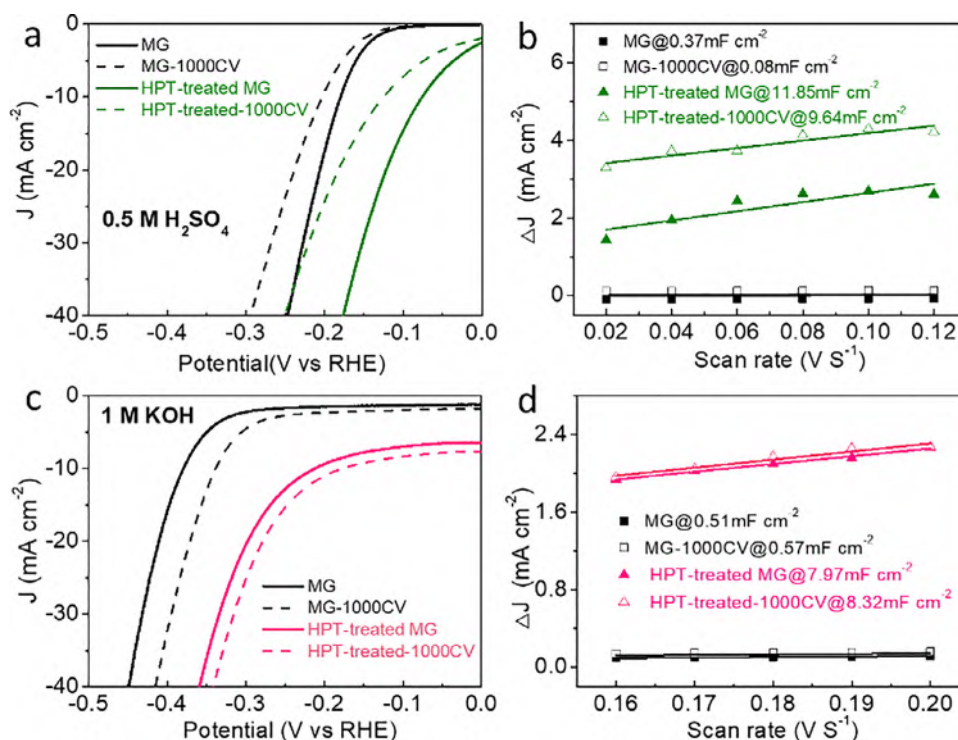
Fig. 2. LSV curves and the capacitive current density from double layer charging of the melt-spun and HPT-treated $Pd_{40}Cu_{30}Ni_{10}P_{20}$ MGs before and after 1000 CV cycles in (a and b) acidic and (c and d) alkaline electrolytes.

uid region. The structural relaxation of MGs is accelerated during heating, which can be characterized by exothermic or endothermic peaks below T_g in the DSC curves.

The heat release or absorption during this process is an indicator of energy state of MGs [25], which is closely related with the fraction of flow units [26]. As shown in Fig. 1e, the MG has relaxed to a low energy state, characterized by an endothermic peak below T_g. However, the sample was rejuvenated to a higher energy state after HPT with an obvious exothermic peak below T_g. The energy difference between MG and HPT-treated sample was estimated to be 21.7 J/g, which is much larger than that induced by thermal cycling [27], shot peening [28] or high-pressure annealing [26], indicating that a large amount of flow units have been introduced by HPT treatment.

For clearly understanding the energy state changes, a schematic diagram has drawn as shown in Fig. 1f. The HPT treatment introduces more flow units to the amorphous matrix, so that the potential energy of MG is increased and reached a higher and unstable state. Hence, the crystallization behavior is more easily to occur for the HPT-treated MG and this explains the reduction of T_x.

HER performances in acidic and alkaline media of the melt-spun and HPT-treated $Pd_{40}Cu_{30}Ni_{10}P_{20}$ MGs are studied by LSV curves and C_{dl} curves as shown in Fig. 2. At the current density of 10 mA cm^{-2}, the overpotentials of the HPT-treated sample decreases from 179 mV to 76 mV in 0.5 M H_2SO_4 and from 379 mV to 209 mV in 1 M KOH. Different from the melt-spun ribbon, the LSV of the HPT-treated MG shows a current density away from 0 mA cm^{-2} at 0 V. Because the morphology and thickness of the HPT sample and the melt-spun sample are different, it should be clarified whether the phenomenon is related to morphologies or not. The HPT-treated MG was polished to greatly change its surface morphology and thickness. Fig. S2 shows that the cracks and unevenness on the surface disappeared after polishing. The thickness of the sample after two polishing processes is 0.56 mm and 0.48 mm, respectively. Fig. S3 shows the LSV curves of the HPT-treated

MG before and after polishing, which are almost the same. It is thus suggested that the measurement results of LSV is not due to the surface morphology or thickness, but an intrinsic phenomenon of the HPT-treated samples [21].

As shown in Fig. S4, the Tafel slopes of the MG increase after HPT treatment both in acidic and alkaline media, and this might be due to the uneven surface caused by severe plastic deformation. Fig. 2b and d show the capacitive current density from double layer charging of the two samples in acidic and alkaline electrolytes, respectively. The calculated C_{dl} and ESCA are listed in Table 2, where the ECSA of the MG is increased by more than 10 folds upon HPT. These results show that the HER catalytic ability of the melt-spun $Pd_{40}Cu_{30}Ni_{10}P_{20}$ MG can be significantly enhanced by HPT.

For both two samples, the overpotential at 10 mA cm^{-2} increases after 1000 CV cycles in acidic media, however, it decreases in alkaline media. The phenomena should be further clarified. Fig. 3 shows the XPS patterns of Ni $2p$ and P $2p$. Fig.3a-b show that the peaks of Ni^{2+} and P^{5+} of the melt-spun and HPT-treated MGs greatly decreased after 1000 CV cycles in acidic electrolyte. However, as shown in Fig.3c-d, the relative intensity of Ni^{2+} and P^{5+} peaks increased and the P^{3+} peak nearly disappeared after 1000 CV cycles in alkaline media, indicating that a large amount of P^0 has been transformed to P^{5+}. It can be concluded that during the HER process in alkaline electrolyte, the P element and Ni element were combined in the form of Ni_5P_2, which is beneficial for the catalytic performance. As for the acidic situation, not only there is no formation of Ni_5P_2 but also Ni^{2+} falls into the electrolyte. Therefore, the HER performance has a certain degree of degradation after 1000 CV cycles. It is revealed that the HER performance of $Pd_{40}Cu_{30}Ni_{10}P_{20}$ MG after HPT treatment has been improved considerably both in acidic and alkaline media. On the one hand, this is attributed to the microcracks and folds on the sample surface brought by HPT treatment, which increases the effective contact area with the electrolyte (as shown in Fig. 1c and Table 2). Previ-

Table 2

Impedance, overpotentials, Tafel slopes, C_{dl} and ECSA of the melt-spun and HPT-treated $Pd_{40}Cu_{30}Ni_{10}P_{20}$ MGs before and after 1000 CV cycles in acidic and alkaline electrolytes.

Ba	Electrolyte	R_s (ohm cm^2)	R_{ct} (ohm cm^2)	η (mV) at 10 mA cm^{-2}	Tafel slope (mV dec^{-1})	C_{dl} (mF cm^{-2})	ECSA
MG	0.5 M H$_2$SO$_4$	5.83	48.68	179	55	0.37	9.25
	1 M KOH	5.44	100.2	379	102	0.52	13
MG-1000CV	0.5 M H$_2$SO$_4$	5.62	44.24	203	61	0.08	2
	1 M KOH	5.73	119.4	337	103	0.57	14.25
HPT-treated MG	0.5 M H$_2$SO$_4$	4.75	28.22	76	91	11.85	296.25
	1 M KOH	4.21	104.79	209	202	7.97	199.25
HPT-treated-	0.5 M H$_2$SO$_4$	4.24	33.98	125	110	9.64	241
1000CV	1 M KOH	3.57	120.92	174	207	8.32	208
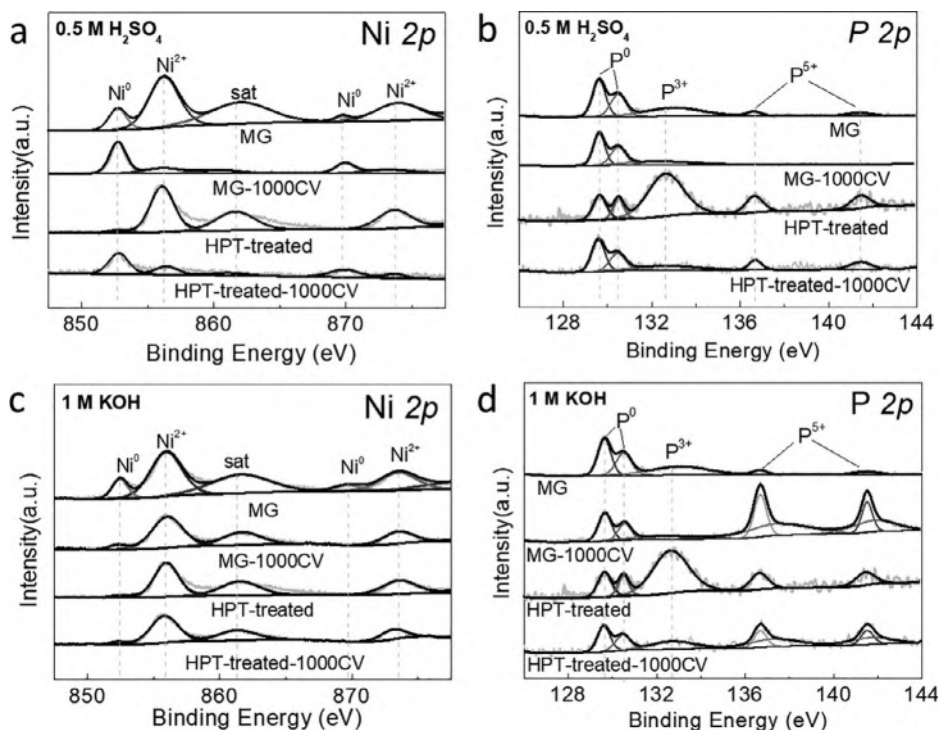
Fig. 3. XPS patterns of Ni *2p* and P *2p* of the melt-spun and HPT-treated $Pd_{40}Cu_{30}Ni_{10}P_{20}$ MGs before and after 1000 CV cycles in (a and b) acidic and (c and d) alkaline electrolytes.
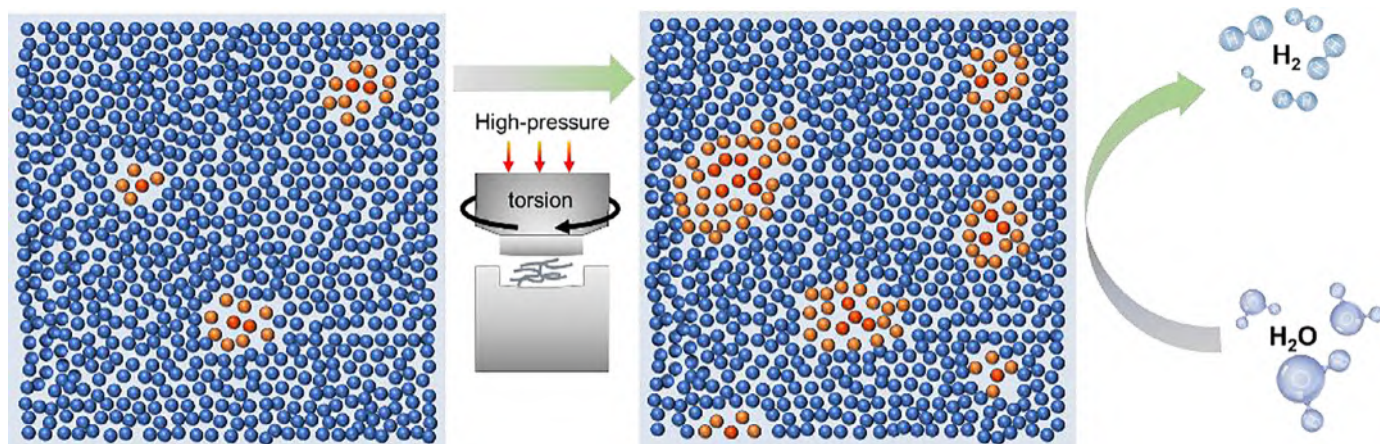

Fig. 4. Schematic diagram of the density of flow units in the amorphous matrix before and after HPT treatment and the hydrogen generation process.

ous studies established that the atomic distribution of MG has a high degree of uniformity in nanoscale.[29,30] However, the AFM images of the HPT-treated sample show compositional heterogeneity in the nanoscale, which may reflect the increased density of flow units (Fig. S9). Additionally, the DSC results in Fig. 1 can also

prove the increase of the quantities of flow units after the HPT treatment. A schematic diagram as shown in Fig. 4 is drawn to illustrate this internal atomic change before and after HPT treatment more intuitively. The density of flow units tremendously increases after HPT processing. The atomic arrangement of these flow unit

areas is looser and has more active sites for HER, and the property of higher energy is more beneficial for the adsorption of H^+ and the generation of H_2.

In summary, this study shows that the severe plastic deformation by HPT treatment can effectively improve the HER performances of a melt-spun $Pd_{40}Cu_{30}Ni_{10}P_{20}$ MG both in acidic and alkaline media, which should be due to the significantly increased density of flow units in the amorphous matrix. The overpotentials at 10 mA cm^{-2} of the HPT-treated $Pd_{40}Cu_{30}Ni_{10}P_{20}$ MG are 76 mV and 209 mV in 0.5 M H_2SO_4 and 1.0 M KOH respectively, which are smaller than 179 mV and 379 mV for the melt-spun $Pd_{40}Cu_{30}Ni_{10}P_{20}$ MG at the same conditions.

Funding

Supplementary information

mmc1.docx

Declaration of Competing Interest

The authors declare no conflict of interest.

Supplementary materials

Supplementary material associated with this article can be found, in the online version, at doi:10.1016/j.scriptamat.2021.114145.

References

[1] C.C.L. McCrory, S. Jung, I.M. Ferrer, S.M. Chatman, J.C. Peters, T.F. Jaramillo, J. Am. Chem. Soc. 137 (13) (2015) 4347–4357.

[2] B.P. Setzler, Z. Zhuang, J.A. Wittkopf, Y. Yan, Nat. Nanotechnol. 11 (12) (2016) 1020–1025.

[3] K. Zeng, D. Zhang, Prog. Energy Combust. Sci. 36 (3) (2010) 307–326.

[4] Y. Zheng, Y. Jiao, M. Jaroniec, S.Z. Qiao, Angew. Chem. Int. Ed. 54 (1) (2015) 52–65.

[5] M.M. Trexler, N.N. Thadhani, Prog. Mater Sci. 55 (8) (2010) 759–839.

[6] Z. Jia, J.C. Wang, S.X. Liang, W.C. Zhang, W.M. Wang, L.C. Zhang, J. Alloys Compd. 728 (2017) 525–533.

[7] F. Hu, S. Zhu, S. Chen, Y. Li, L. Ma, T. Wu, Y. Zhang, C. Wang, C. Liu, X. Yang, Adv. Mater. 29 (32) (2017) 1606570.

[8] J.Q. Wang, Y.H. Liu, M.W. Chen, G.Q. Xie, D.V. Louzguine-Luzgin, A. Inoue, J.H. Perepezko, Adv. Funct. Mater. 22 (12) (2012) 2567–2570.

[9] Y.C. Hu, Y.Z. Wang, R. Su, C.R. Cao, F. Li, C.W. Sun, Y. Yang, P.F. Guan, D.W. Ding, Z.L. Wang, Adv. Mater. 28 (46) (2016) 10293–10297.

[10] Wang W., Sci. China Phys. Mech. 44 (4) (2014) 396–405.

[11] P.S. Salmon, Nat. Mater. 1 (2) (2002) 87–88.

[12] H. Wagner, D. Bedorf, S. Kuechemann, M. Schwabe, B. Zhang, W. Arnold, K. Samwer, Nat. Mater. 10 (6) (2011) 439–442.

[13] R. Xue, D. Wang, Z. Zhu, D. Ding, B. Zhang, W. Wang, J. Appl. Phys. 114 (12) (2013) 123514.

[14] A. Inoue, Acta Mater. 48 (1) (2000) 279–306.

[15] A. Madan, M.P. Shaw, The Physics and Applications of Amorphous Semiconductors, Elsevier, 2012.

[16] Z. Wang, W.-H. Wang, Natl. Sci. Rev. 6 (2) (2019) 304–323.

[17] A.P. Zhilyaev, T.G. Langdon, Prog. Mater Sci. 53 (6) (2008) 893–979.

[18] G. Rogl, D. Setman, E. Schafler, J. Horky, M. Kerber, M. Zehetbauer, M. Falmbigl, P. Rogl, E. Royanian, E. Bauer, Acta Mater. 60 (5) (2012) 2146–2157.

[19] S.C. Yoon, Z. Horita, H.S. Kim, J. Mater. Process. Technol. 201 (1-3) (2008) 32–36.

[20] K. Edalati, E. Akiba, Z. Horita, Sci. Technol. Adv. Mater. 19 (1) (2018) 185–193.

[21] K. Wu, Y. Meng, J. Xu, K. Edalati, H. Shao, W. Li, H.-J. Lin, Scr. Mater. 188 (2020) 135–139.

[22] K. Wu, F. Chu, Y. Meng, K. Edalati, Q. Gao, W. Li, H.-J. Lin, J. Mater. Chem. A 9 (2021) 12152–12160.

[23] B. Conway, B. Tilak, Electrochim. Acta 47 (22-23) (2002) 3571–3594.

[24] F. Chu, K. Wu, Y. Meng, K. Edalati, H.-J. Lin, Int. J. Hydrogen Energy 46 (49) (2021) 25029–25038 in press.

[25] M. Stolpe, J. Kruzic, R. Busch, Acta Mater. 64 (2014) 231–240.

[26] C. Wang, Z. Yang, T. Ma, Y. Sun, Y. Yin, Y. Gong, L. Gu, P. Wen, P. Zhu, Y. Long, Appl. Phys. Lett. 110 (11) (2017) 111901.

[27] S. Ketov, Y. Sun, S. Nachum, Z. Lu, A. Checchi, A. Beraldin, H. Bai, W. Wang, D. Louzguine-Luzgin, M. Carpenter, Nature 524 (7564) (2015) 200–203.

[28] A. Concustell, F. Méar, S. Surinach, M. Baró, A. Greer, Philos. Mag. Lett. 89 (12) (2009) 831–840.

[29] Y. Yang, J. Zeng, A. Volland, J. Blandin, S. Gravier, C.T. Liu, Acta Mater. 60 (13-14) (2012) 5260–5272.

[30] H.-J. Lin, M. He, S.-P. Pan, L. Gu, H.-W. Li, H. Wang, L.-Z. Ouyang, J.-W. Liu, T.-P. Ge, D.-P. Wang, Acta Mater. 120 (2016) 68–74.